



Contribution of components from volume defect in natural pyrite and quartz to solution chemistry of flotation pulp

Yong-jun XIAN¹, Qi NIE², Shu-ming WEN¹, Yi-jie WANG¹

1. State Key Laboratory of Complex Nonferrous Metal Resources Clean Utilization, Kunming University of Science and Technology, Kunming 650093, China;
2. Faculty of Mining Engineering, Kunming Metallurgy College, Kunming 650033, China

Received 15 August 2014; accepted 1 July 2015

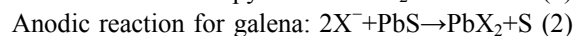
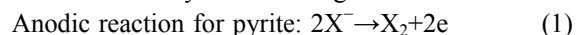
Abstract: The volume defects in pure pyrite and quartz from a classical Cu–Pb–Zn–Fe sulfide deposit were investigated. The results indicate that a large number of volume defects exist in natural pyrite and quartz. The volume defects assume a variety of shapes, including long strips, oval shapes and irregular shapes, with sizes ranging from a few microns to dozens of microns. These volume defects are rich in metallogenic elements as a result of the capture of metallogenic and mineralizing fluid during the defect-forming process. The volume defects are fractured during the grinding process, and their chemical components are released into the solution, as confirmed by the abundant presence of various metal and non-metal components in the cleaning water and EDS results. Under the experimental conditions of 10 g pyrite or quartz with grinding fineness of $d_{90}=37\ \mu\text{m}$, which was cleaned in 40 mL of pure deionised water under an inert atmosphere, the total average concentrations of Cu, Pb, Zn, Fe, Ca, Mg and Cl^- in the aqueous solution are 32.09×10^{-7} , 16.51×10^{-7} , 19.45×10^{-7} , 516.52×10^{-7} , 129.50×10^{-7} , 35.30×10^{-7} and 433.80×10^{-7} mol/L, respectively, for pyrite and 19.20×10^{-7} , 8.88×10^{-7} , 8.31×10^{-7} , 82.71×10^{-7} , 16.21×10^{-7} , 4.28×10^{-7} and 731.26×10^{-7} mol/L, respectively, for quartz. These values are significantly greater than those from the experimental non-oxidative dissolution of the pyrite or quartz, respectively. Therefore, the metallogenic fluid in volume defects of mineral crystal is concluded to represent the dominant contribution to the solution chemistry of sulfide flotation pulp. The present investigation will help to deeply understand the flotation theory of sulfide minerals.

Key words: pyrite; quartz; volume defect; metallogenic fluid; component release

1 Introduction

Froth flotation is a widely used method for the beneficiation or separation of complex sulfide minerals in industry. However, the flotation practice shows that the floatability of sulfides from various deposits and even from different diggings in one deposit is very different, which often leads to unsatisfactory effectiveness of separation of the complex sulfides by flotation. In order to solve this problem, many experimental studies on the flotation performance of sulfide minerals have been performed using various analytic and testing technologies in the past several decades. It has been well known that most of the sulfides are semiconducting minerals with narrow band gap and their flotation process closely involves electrochemical

reactions. In the process of sulfide flotation, it has been well proved that oxygen accepts electrons on the sulfide surface on which the cathodic reaction occurs, while xanthate (X^-) loses electrons on the sulfide surface on which the anodic reaction occurs. The above processes can be summarized by the following redox reactions:



From Reactions (1)–(3), the rest potential of sulfide electrode predominantly affects the electrochemical reaction on sulfide surface [1–5].

As we know, perfect mineral crystal does not exist in nature. Even under absolute zero condition, the crystal defect is also impossible to be avoided. During the ore-forming, the lattice defect of sulfide always results from the loss of its anions or cations, causing

vacancy defect. In addition, the extraneous ions such as Pb, Cu, Se, Zn, Au and Ag ions, substitute for lattice sites or occupy interstitial void of sulfide crystal. In recent years, some researchers have proposed that the lattice defects in the sulfide crystal change the electrochemical properties of the mineral and impact the electrochemical processes, which vary floatability of sulfide from different areas during flotation [6]. SUN et al [7] reported that the lattice substitution of Cu and Fe ions in sphalerite resulted in increasing the surface free-electrons and the electro-chemical activity of sphalerite. In the study of the density functional theory (DFT), LI et al [8] found that vacancy defects significantly influenced the covalence and electrochemical properties of pyrite and adversely affected pyrite flotation. In a series of experiments, CHEN et al [9–11] studied the effect of lattice substitution on electronic structures and flotation behaviors of sphalerite, and the results showed that the lattice substitution of Mn, Fe, Ni, Cu, Sn and Pb ions in sphalerite benefited the adsorption of O₂ and xanthate. CHEN et al [12] reported that the lattice substitution of Sb and Mn ions led to the over-oxidation of galena, which is unfavorable for the flotation of galena. In a series of experiments, it is demonstrated that the presence of Co, As and Ni ions in pyrite results in the semiconductor type conversion of pyrite and influences the oxidation of the pyrite surface under moist-air conditions [13–15]. These studies provide valuable background and methods for understanding the correlation between lattice defects and flotation behavior of sulfides. However, some important science issues remain unresolved. In fact, during the ore-forming, beside the above-mentioned lattice defects (point defects), the natural mineral crystal also contains many volume defects formed through growing and extending the point defects to three-dimensional defects. So far, there has been little discussion on the correlation between the volume defects and the floatability of sulfides.

The geochemistry knowledge represents that mass metallogenic fluid has been trapped and closed in volume defects of minerals of hydrothermal ore deposits which often precipitate as sulfides in abundance from hot metal-rich fluid passing through small porous or fractured rocks [16]. This implies that the metallogenic fluid in volume defects may contain active metal ions due to their ability of carrying metal metallogenic ions during ore formation. Once the ores are crushed and ground during the mineral liberation processing, the volume defects in the minerals are deteriorated and their chemical components are released into the flotation pulp, which significantly influence the solution chemistry of the flotation pulp and the surface properties of sulfide minerals, as well as the flotation performance of

metal–sulfide minerals. However, there are few reports about the characterization of volume defects in mineral crystal. Hence, in this work, the characterization of volume defects formed in pyrite and its closely associated quartz was investigated, and the concentrations of various components released from the volume defects were determined. The results would be helpful for the understanding of flotation solution chemistry.

2 Experimental

2.1 Description of deposit and material

The material used in the present investigation was from a Cu–Pb–Zn–Fe sulfide deposit at Dapingzhang in the Lancangjiang River zone of Southwest Yunnan Province in China. This deposit is an important representative of a large volcanogenic hydrothermal sedimentary deposit and occurs as polymetallic massive sulfide mineralization mainly containing pyrite, sphalerite, galena, chalcopyrite and tetrahedrite–tennantite metal mineral. The gangue is mainly composed of quartz and small amounts of calcite and barite [17].

Twelve representative bulk-rock samples were chosen for the metallogenic fluid-release tests. The samples were crushed into +0.5–1 mm particles, and the high-purity pyrite and quartz crystals liberated from the sulfides were hand-picked under a microscope. The chemical analysis of the materials showed that the pyrite contained 44.06% Fe and 54.57% S, and the quartz contained 98.35% SiO₂. An X-ray diffraction (D/Max 2200, Rigaku, Japan) analysis of the pyrite and quartz demonstrated that their high purity with no apparent impurities.

2.2 IUM characterization of volume defect

Pure pyrite or quartz bulk was cut into thin slices with a thickness of 1 mm, and the slices were doubly polished. The morphology of volume defect was observed through an infrared-ultraviolet microscope (IUM, BX51, USA). The information obtained from the microscope observation was converted into a data signal using infrared electronic induction, and the data signal was subsequently treated using computer software to produce an output picture.

2.3 HRXMT characterization of volume defect

High resolution X-ray micro tomography (HRXMT) with cone-beam and micro-computed tomography (CT) system was introduced to investigate granular pyrite. Cone-beam X-ray micro-tomography [18,19] offers a unique imaging capability which can produce three-dimensional images of the internal structure of samples

with micrometer resolution. Rather than rotating the X-ray source and detectors during data collection, in medical CT technology, the specimen is rotated. Instead of generating a series of two-dimensional sliced images from one-dimensional projections, a three-dimensional reconstruction image array is created directly from two-dimensional projections. Details for the description of this micro-CT system and its corresponding reconstruction algorithm can be found in Ref. [20].

The sample was evenly separated, prepared, and sealed in a syringe tube for HRXMT scanning. The pyrite sample, which had the highest density, was scanned for 4 h under 150 kV to obtain sufficient X-ray intensity.

2.4 SEM–EDS characterization of fracturing position of volume defect

The morphology of the fracturing positions of volume defect on pyrite surface was observed using a scanning electron microscope (SEM, Philip XL30) operated at accelerating voltages of 0.5–30 kV and equipped with a spectrometer for microanalysis based on an energy dispersive X-ray spectroscopy system (EDS).

2.5 Measurement of various components in volume defects

Purging with Ar produced deoxygenated deionized water. The effectiveness of the Ar purging was confirmed with a dissolved-O₂ probe with high sensitivity. After 1 h of Ar purging, the water contained dissolved O₂ with content less than 1×10^{-6} . The material was washed with deoxygenated 0.1 mol/L H₂SO₄ solution, and then rinsed 30 times with deoxygenated deionized water with conductivity less than 18.0 mS/m and air-dried. The material was subsequently dry-ground in an agate cup mill (MM400, Retsch, Germany) for 10 min at a frequency of 15 s^{-1} for subsequent experiments, and the particle size of the final sample was $d_{90}=37 \text{ }\mu\text{m}$. Next, 10 g ground material and 40 mL deoxygenated deionized water were added to a centrifuge tube and ultrasonically cleaned for 1 min. When this cleaning process was completed, a centrifuge was used for solid–liquid separation. The supernatant from the separation was stored in closed vials and analyzed for the total concentration of Cu, Pb, Zn, Fe, Ca and Mg by inductively coupled plasma–atomic emission spectrometry plasma–mass spectrometry (ICP–MS, ELAN–DRCII, PE, USA) and Cl[−] by ion chromatography (IC, 820–413, Waters, USA); the solid from the separation was collected and rinsed with pure deionized water and subsequently used for dissolution experiments.

All of the previously described experimental processes were operated in an oxygen-free glove box (i.e., argon-saturated atmosphere) to avoid contamination

by atmospheric oxygen. The experiments were performed at room temperature of 25 °C. Each experiment was repeated three times, and the average value was obtained.

2.6 Non-oxidative dissolution of material in pure deionized water

The non-oxidative dissolution processes were also performed in an oxygen-free glove box at room temperature of 25 °C. After the step of Section 2.5, the air-dried solid and 40 mL deoxygenated deionized water were added to a glass reactor and rapidly stirred (400 r/min) with a magnetic stirrer for 5 h. When the dissolution experiment was completed, a centrifuge was used for solid–liquid separation; the supernatant from the separation was stored in closed vials and analyzed for the total concentration of Cu, Pb, Zn, Fe, Ca and Mg by ICP–MS and for the total concentration of Cl[−] by IC.

3 Results and discussion

3.1 IUM characterization of volume defect in pyrite and quartz

The morphologies of volume defects in pyrite and quartz obtained using IUM microscopy are shown in Fig. 1. Due to the immaturity of the technology and the

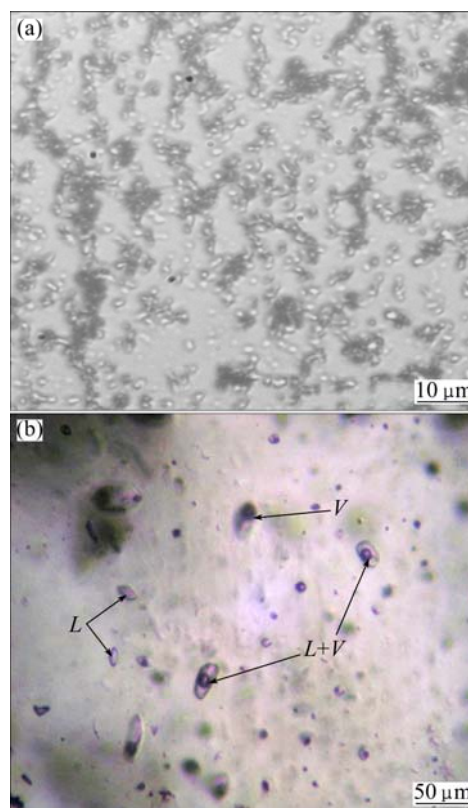


Fig. 1 Micrographs of volume defects in pyrite (a) and quartz (b): L—Pure liquid phase; V—Pure gaseous phase; V+L—Gas–liquid mixed phases

poor transparency of pyrite [21], only volume defects in superficial layers of pyrite can be observed (Fig. 1(a)). As shown in Fig. 1(a), different compositions between relatively light and dark regions are easily recognized. These different regions resulted from the differences between the components of the volume defect and minerals, or between the substances formed via a chemical reaction of the volume defect and the minerals, which absorbed different infrared-ultraviolet wavelengths of light and resulted in dark regions in the image.

In comparison with pyrite, the morphology of the volume defects in the quartz internal crystal structure was easily observed using an IUM microscope (Fig. 1(b)) because quartz had good transparency. In Fig. 1(b), many volume defects with long, oval and irregular shapes were observed, and they were isolated or in groups in the quartz crystal; the sizes of these volume defects ranged from a few microns to dozens of microns. Moreover, most of volume defects in quartz were mainly filled with pure gas, pure liquid or gas-liquid mixed phases. The gas phases were mainly composed of CO₂, CH₄, N₂, H₂, O₂ and inert gases, while the liquid phases were composed of metallogenic fluid [16].

3.2 HRXMT characterization of volume defect in pyrite

HRXMT can produce multi-dimensional images of the internal crystal structure of samples with micrometer resolution [22]. The HRXMT image represents thousands of particles simultaneously, thus facilitating revealing the volume defect structures in pyrite crystal. The results are shown in Fig. 2.

The HRXMT image (Fig. 2(a)) shows that there are numerous void (Positions 1 and 3) and crack (Position 2) defects ranged from dozens microns to one hundred microns in the pyrite crystal. From the micro-CT scan graph (Fig. 2(c)), it can be seen that the internal crystal of pyrite is porous. This result is consistent with the IUM result. Both confirm the existence of volume defect.

3.3 SEM-EDS characterization for fracture position of volume defect on pyrite surface

The surface morphologies of the polished pyrite and quartz slices are shown in Fig. 3. From the Figs. 3(a) and (b), there are numerous “hollows” on the pyrite surface, and they may be attributed to the fracturing of the volume defects. Based on the direct SEM observation of the structure and morphology of the “hollows”, the inclusions clearly exhibit different shapes with sizes of a few microns. Some of the inclusions exhibit strip, elliptical, ball shapes or irregular shapes. With respect to the inclusion structure and state, the results obtained

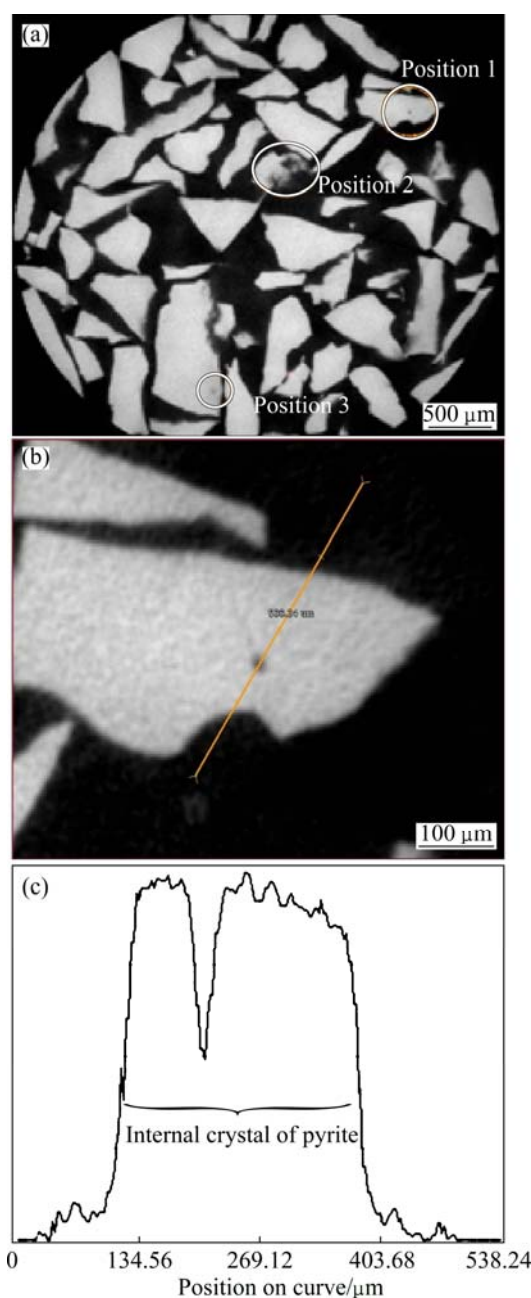


Fig. 2 HRXMT image of pyrite: (a) Three-dimensional image at relatively low magnification; (b) Position 1 in (a) at high magnification; (c) Micro-CT scan graph of line in (b)

using SEM morphology analysis agree with the results obtained from the infrared optical microscopic images of volume defects in pyrite and quartz.

To prove that the “hollows” present on the surface are the result of volume defect fracturing, rather than scratches during slicing preparation, EDS analysis was performed at the positions of the “hollows”. For comparison, region and point analyses were performed in the flat region (Region 4) around the “hollows” region (Positions 1, 2 and 3), as shown by the marks in Fig. 3(b). The corresponding EDS results (i.e., the elemental contents based on semi-quantitative analysis) are shown

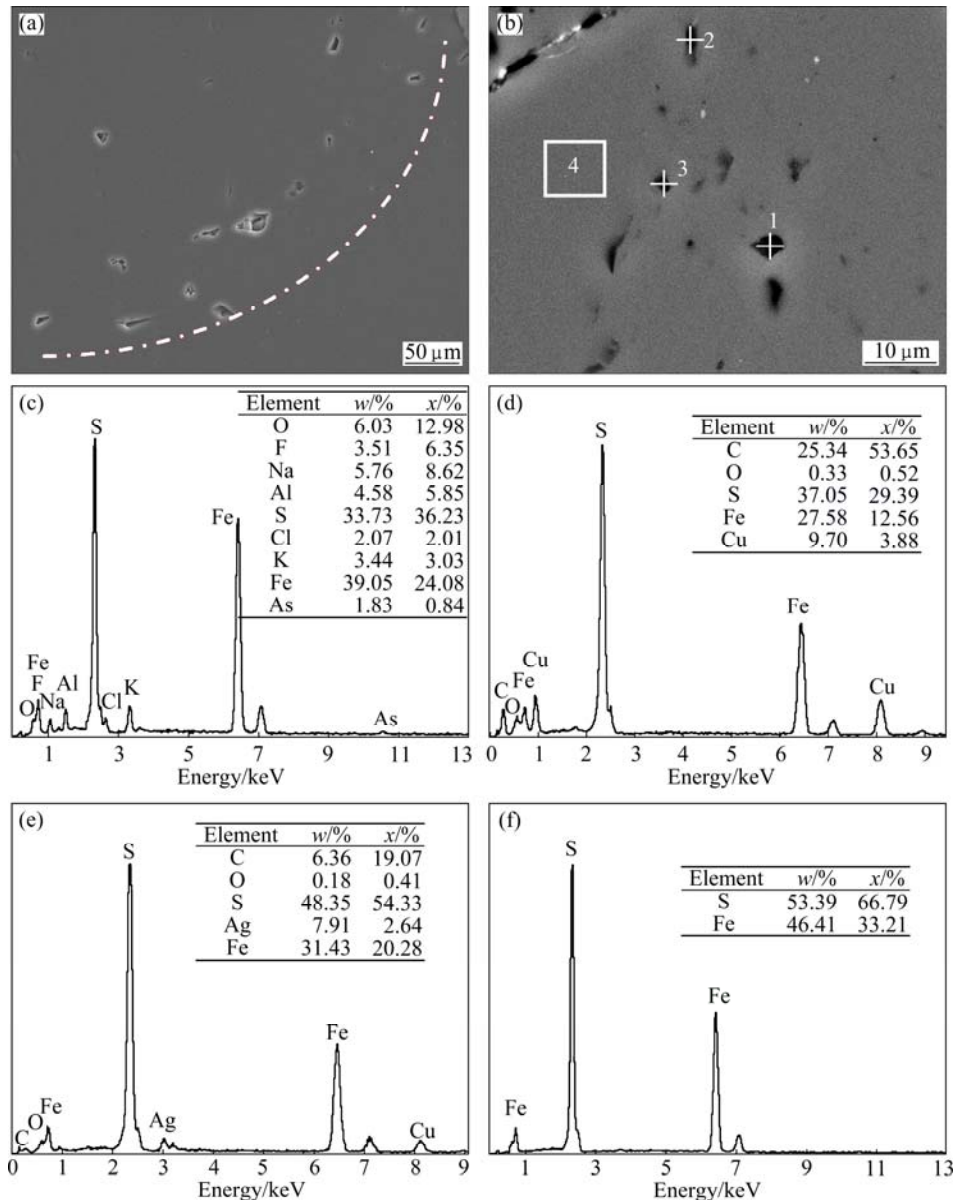


Fig. 3 Secondary electron image (a) and backscattered electron image (b) of pyrite surface, and EDS results of Position 1 (c), Position 2 (d), Position 3 (e) and Region 4 (f)

in Figs. 3(c)–(f). The signals of C, O, K, Na, Ca, Mg, Al, Cu, As and Ag were detected at the position of the “hollows”. Notably, Cl and F at Position 1 provide powerful evidence for the fact that these regions represent fractured volume defects, due to the fact that Cl and F are the most commonly occurring elements in metallogenic fluid of hydrothermal deposit [23]. In addition, the mole ratios of the namesake ions (i.e., $n(\text{S})/n(\text{Fe})$) at Positions 1, 2 and 3 deviate the theoretical value of 2:1. However, only the peaks of S and Fe are presented in the electron spectrum acquired in Region 4 in Fig. 3(f), in which the mole ratio of S to Fe is very close to the stoichiometry of pyrite FeS_2 (2:1). The EDS results indicate that the compositions of the “hollow” positions differ from those of the flat area; therefore, the “hollows” were caused by the fracturing of volume

defects rather than by scratches of the surface. The change in composition originated from the release of the volume defects. The “hollows” were preserved after the volume defects fractured, and multiple ions in the volume defects were adsorbed onto the defect–mineral interface after the gas phase and liquid phase were volatilized.

3.4 Concentration of ions in pyrite volume defect

In this section, a series of parallel tests on the release of volume defects were performed. ICP–MS and IC were used to measure the concentrations of Cu, Pb, Zn, Fe, Ca, Mg and Cl^- , respectively, released from pyrite and quartz volume defects during the grinding process. The results are summarized in Table 1. Based on the results in Table 1, after the samples were

Table 1 Concentrations of various components in aqueous solution

Test step	Material	Concentration/(10^{-7} mol·L $^{-1}$)						
		Cu	Pb	Zn	Fe	Ca	Mg	Cl $^{-}$
Cleaning	Pyrite	32.09	16.51	19.45	516.52	129.50	35.30	433.80
	Quartz	19.20	8.88	8.31	82.71	16.21	4.28	731.26
Non-oxidative dissolution	Pyrite	0.23	0.004	<LOD	11.12	0.052	0.26	17.38
	Quartz	0.19	<LOD	<LOD	9.97	0.10	0.005	42.73

LOD means limit of detection. The lowest LODs of ICP-MS and IC are about 1×10^{-9}

ultrasonically cleaned for 1 min, the average concentrations of Cu, Pb, Zn, Fe, Ca, Mg and Cl $^{-}$ were 32.09×10^{-7} , 16.51×10^{-7} , 19.45×10^{-7} , 516.52×10^{-7} , 129.50×10^{-7} , 35.30×10^{-7} and 433.80×10^{-7} mol/L, respectively, for pyrite and 19.20×10^{-7} , 8.88×10^{-7} , 8.31×10^{-7} , 82.71×10^{-7} , 16.21×10^{-7} , 4.28×10^{-7} and 731.26×10^{-7} mol/L, respectively, for quartz. Although the conditions for each test were constant, the concentrations of Cu, Pb, Zn, Fe, Ca, Mg and Cl $^{-}$ in the cleaning water from each test are comparatively unstable. This instability arises because the distributions of volume defects in minerals and the concentrations of Cu, Pb, Zn, Fe, Ca, Mg and Cl $^{-}$ in these volume defects are asymmetrical and random.

To eliminate the possibility that Cu, Pb, Zn, Fe, Ca, Mg and Cl $^{-}$ in the solution originated from the dissolution of minerals, which existed but were difficult to be detected, mineral samples cleaned for 1 min were then non-oxidatively dissolved for 5 h in a glove box with argon gas protection and in a cleaned beaker. Compared with the concentrations of Cu, Pb, Zn, Fe, Ca, Mg and Cl $^{-}$ in the cleaning water, the concentrations after non-oxidative dissolution were lower by up to two orders of magnitude. Thus, the abundance of Cu, Pb, Zn, Fe, Ca, Mg and Cl $^{-}$ in the cleaning water can most likely be attributed to the release of metallogenic fluid filled in volume defects rather than from the mineral dissolution, and the chemical components released from volume defects of the mineral are import sources of the “unavoidable ions” in solution. The present investigation provides a new understanding regarding the source of “unavoidable ions” in solution and would also be of significant importance to flotation theory of sulfides.

4 Conclusions

1) Microscopic observations by IUM and HRXMT show that large numbers of volume defects with sizes varying from a few microns to hundreds of microns exist in samples of natural pyrite and are closely associated quartz. The volume defects are mainly filled in metallogenic fluid. SEM-EDS analyses indicate that the regions of the fracturing volume defects differ in morphology and chemical composition from those of the

flat area, and that numerous alkali metallic elements and metallogenic element of varying concentrations are present in the regions of the fracturing volume defects.

2) The metallogenic fluid in volume defects of pyrite and quartz carries various chemical components, such as Cu, Pb, Zn, Fe, Ca, Mg and Cl $^{-}$, and is released to the solution during the grinding process. The metal and non-metal components released from the volume defects of pyrite and quartz provide a new source of ions in flotation pulp.

Acknowledgments

Helpful technical supports from the State Key Laboratory for Mineral Deposit Research Institute of Geo-Fluids at Nanjing University and the Department of Metallurgical Engineering at University of Utah (HRXMT) are gratefully acknowledged.

References

- [1] WOODS R. Oxidation of ethyl xanthate on platinum, gold, copper, and galena electrodes: Relation to the mechanism of mineral flotation [J]. *The Journal of Physical Chemistry*, 1971, 75(3): 354–362.
- [2] ALLISON S A, GOOLD L A, NICOL M J, GRANVILLE A. A determination of the products of reaction between various sulfide minerals and aqueous xanthate solution, and a correlation of the products with electrode rest potentials [J]. *Metallurgical Transactions*, 1972, 3(10): 2613–2618.
- [3] KOWAL A, POMIANOWSKI A. Cyclic voltammetry of ethyl xanthate on a natural copper sulphide electrode [J]. *Journal of Electroanalytical Chemistry and Interfacial Electrochemistry*, 1973, 46(2): 411–420.
- [4] GARDNER J R, WOODS R. Electrochemical investigation of contact angle and of flotation in the presence of alkylxanthates. II: Galena and pyrite surfaces [J]. *Australian Journal of Chemistry*, 1977, 30(5): 981–991.
- [5] RALSTON J. The chemistry of galena flotation: Principles & practice [J]. *Mineral Engineering*, 1994, 7(5–6): 715–735.
- [6] ABRAITIS P K, PATTRICK R A D, VAUGHAN D J. Variations in the compositional, textural and electrical properties of natural pyrite: A review [J]. *International Journal of Mineral Processing*, 2004, 74(1–4): 41–59.
- [7] SUN Wei, HU Yue-hua, QIN Wen-qing. DFT research on activation of sphalerite [J]. *Transactions of Nonferrous Metals Society of China*, 2004, 14(2): 376–382.
- [8] LI Y Q, CHEN J H, CHEN Y. Electronic structures and flotation behavior of pyrite containing vacancy defects [J]. *Acta Physico-Chimica Sinica*, 2010, 26(5): 1435–1441.

- [9] CHEN Y, CHEN J H, GUO J. A DFT study on the effect of lattice impurities on the electronic structures and floatability of sphalerite [J]. Minerals Engineering, 2010, 23(14): 1120–1130.
- [10] CHEN Jian-hua, CHEN Ye, LI Yu-qiong. Effect of vacancy defects on electronic properties and activation of sphalerite (110) surface by first-principles [J]. Transactions of Nonferrous Metals Society of China, 2010, 20(3): 502–506.
- [11] CHEN J H, CHEN Y. A first-principle study of the effect of vacancy defects and impurities on the adsorption of O₂ on sphalerite surfaces [J]. Colloids and Surfaces A: Physicochemical and Engineering Aspects, 2010, 363(1–3): 56–63.
- [12] CHEN J H, WANG L, CHEN Y, GUO J. A DFT study of the effect of natural impurities on the electronic structure of galena [J]. International Journal of Mineral Processing, 2011, 98(3–4): 132–136.
- [13] SAVAGE K S, STEFAN D, LEHNER S W. Impurities and heterogeneity in pyrite: Influences on electrical properties and oxidation products [J]. Applied Geochemistry, 2008, 23(2): 103–120.
- [14] LEHNER S, SAVAGE K, CIOBANU M, CLIFFEL D E. The effect of As, Co, and Ni impurities on pyrite oxidation kinetics: An electrochemical study of synthetic pyrite [J]. Geochimica et Cosmochimica Acta, 2007, 71(10): 2491–2509.
- [15] LEHNER S W, SAVAGE K S, AYERS J C. Vapor growth and characterization of pyrite (FeS₂) doped with Co, Ni, and As: Variations in semiconducting properties [J]. Journal of Crystal Growth, 2006, 286(2): 306–317.
- [16] ROEDDER E, RIBBE P S. Fluid inclusions [M]. Virginia: Mineralogical Society of America, 1984: 1–644.
- [17] LEHMANN B, ZHAO X F, ZHOU M F, DU A D, MAO J W, ZENG P S, FRIEDHELM H K, KLAUS H. Mid-Silurian back-arc spreading at the northeastern margin of Gondwana: The Dapingzhang dacite-hosted massive sulfide deposit, Lancangjiang zone, southwestern Yunnan, China [J]. Gondwana Research, 2013, 24(2): 648–663.
- [18] FELDKAMP L A, DAVIS L C, KRESS J W. Practical cone-beam algorithm [J]. Journal of the Optical Society of America, 1984, 1(6): 612–619.
- [19] LIN C L, MILLER J D. Cone beam X-ray microtomography for three-dimensional liberation analysis in the 21st century [J]. International Journal of Mineral Processing, 1996, 47(1–2): 61–73.
- [20] GONG W X, BERTRAND G. A simple parallel 3D thinning algorithm [C]//Proceedings of the 10th International Conference on Pattern Recognition. New Jersey: Institute of Electrical and Electronic Engineers (IEEE), 1990: 188–190.
- [21] LÜDERS K, ZIEMANN M. Possibilities and limits of infrared light microthermometry applied to studies of pyrite-hosted fluid inclusions [J]. Chemical Geology, 1999, 154(1–4): 169–178.
- [22] LIN C L, MILLER J D. Network analysis of filter cake pore structure by high resolution X-ray microtomography [J]. Chemical Engineering Journal, 2000, 77(1–2): 79–86.
- [23] WILKINSON J J. Fluid inclusions in hydrothermal ore deposits [J]. Lithos, 2001, 55(1–4): 229–272.

天然黄铁矿和石英中体缺陷组分对浮选溶液化学的贡献

先永骏¹, 聂琪², 文书明¹, 王伊杰¹

1. 昆明理工大学 复杂有色金属资源清洁利用国家重点实验室, 昆明 650093;

2. 昆明冶金高等专科学校 矿业学院, 昆明 650033

摘要: 以某一典型 Cu–Pb–Zn–Fe 硫化矿床中的黄铁矿和石英为研究对象, 对其晶体中的体缺陷特征进行研究。结果表明: 天然黄铁矿和石英晶体中存在大量体缺陷, 这些体缺陷呈现各种形态, 包括长条形、椭圆形和不规则形状, 大小从几微米到近百微米不等。由于体缺陷在形成过程中能捕获成矿流体和矿化流体, 因此, 含有大量成矿元素。水溶液的多种金属和非金属化学成分分析及 EDS 分析结果表明, 在磨矿的过程中, 矿物中体缺陷将破裂或断裂, 向溶液中释放其中的化学成分。在磨矿细度为 $d_{90}=37\ \mu\text{m}$, 含 10 g 黄铁矿的 40 mL 清洗溶液中, Cu, Pb, Zn, Fe, Ca, Mg 和 Cl⁻ 的浓度分别达到 32.09×10^{-7} 、 16.51×10^{-7} 、 19.45×10^{-7} 、 516.52×10^{-7} 、 129.50×10^{-7} 、 35.30×10^{-7} 和 433.80×10^{-7} mol/L; 含石英的清洗水溶液中上述离子的浓度分别达到 19.20×10^{-7} 、 8.88×10^{-7} 、 8.31×10^{-7} 、 82.71×10^{-7} 、 16.21×10^{-7} 、 4.28×10^{-7} 和 731.26×10^{-7} mol/L, 此浓度远高于黄铁矿或石英非氧化溶解时相应的浓度。因此, 矿物晶体体缺陷中的成矿流体对硫化矿浮选溶液化学具有重要贡献, 这将有助于深入认识硫化矿浮选的本质。

关键词: 黄铁矿; 石英; 体缺陷; 成矿流体; 组分释放

(Edited by Wei-ping CHEN)